Core@Corona Functional Nanoparticles-driven Rod-Coil Diblock Copolymer Self- Assembly

Coste Mawele Loudy, Joachim Allouche, Antoine Bousquet, Cecile Courreges, Hervé Martinez, Laurent Billon

▶ **To cite this version:**

Coste Mawele Loudy, Joachim Allouche, Antoine Bousquet, Cecile Courreges, Hervé Martinez, et al.. Core@Corona Functional Nanoparticles-driven Rod-Coil Diblock Copolymer Self- Assembly. Langmuir, 2019, 35 (51), pp.16925-16934. 10.1021/acs.langmuir.9b02744 . hal-03006669

HAL Id: hal-03006669
https://hal.science/hal-03006669v1

Submitted on 16 Nov 2020

HAL is a multi-disciplinary open access archive for the deposit and dissemination of scientific research documents, whether they are published or not. The documents may come from teaching and research institutions in France or abroad, or from public or private research centers.

L'archive ouverte pluridisciplinaire **HAL**, est destinée au dépôt et à la diffusion de documents scientifiques de niveau recherche, publiés ou non, émanant des établissements d'enseignement et de recherche français ou étrangers, des laboratoires publics ou privés.

Core@Corona Functional Nanoparticles-driven Rod-Coil Diblock Copolymer Self-Assembly

Coste Mawele Loudy [1,2], Joachim Allouche [1], Antoine Bousquet [1], Cécile Courrèges [1], Hervé Martinez [1], Laurent Billon [1,2]**

[1] CNRS/Université de Pau et des Pays de l'Adour/E2S UPPA, IPREM CNRS-UMR 5254 Hélioparc, 2 avenue Président Angot, 64053 Pau Cedex 9, France

[2] Bio-inspired Materials Group: Functionality & Self-assembly, Université de Pau et des Pays de l'Adour, IPREM CNRS-UMR 5254, Hélioparc, 2 avenue Président Angot, 64053 Pau Cedex 9, France

Corresponding Authors:

Herve.martinez@univ-pau.fr, Laurent.billon@univ-pau.fr

ABSTRACT. Herein, a novel strategy to overcome the influence of $\pi-\pi$ stacking on the rod-coil copolymer organization of is reported. A diblock copolymer poly(3-hexylthiophene)-*block*-poly(ethylene glycol methylether methacrylate) P3HT-*b*-PEGMA was synthesized by a Huisgen cyclo-addition, so-called "Click chemistry", combining the P3HT and PEGMA blocks synthesized by Atom Transfer Radical Polymerization (ATRP) and Kumada Catalyst Transfer Polymerization (KCTP), respectively. Using a dip-coating process, the original film organization of the diblock copolymer was controlled by the crystallization of the P3HT block *via* $\pi-\pi$ stacking. The morphology of the P3HT-*b*-PEGMA films was influenced by the incorporation of gold nanoparticles GNPs coated by Poly(EthyleneGlycol) ligands. Indeed, the crystalline structuration of the P3HT sequence was counterbalanced by the addition in the film of gold nanoparticles finely localized within the copolymer PEGMA matrix. Transmission Electron Microscopy (TEM) and ToF-SIMS analysis validated the GNPs homogeneous localization into the compatible PEGMA phase. Differential Scanning Calorimetry (DSC) showed the rod block crystallization disruption. A morphological transition of the self-assembly is observed by Atomic Force Microscopy (AFM) from P3HT fibrils into *out of plane* cylinders-like driven by the nanophase segregation.

Keywords: click chemistry, rod-coil diblock copolymer, gold nanoparticle, self-assembly, $\pi-\pi$ interactions.

Introduction

Future applications for photovoltaic[1], microelectronic[2,3], or photonic[4] will require the development of new materials with novel and complex properties that pure organic or inorganic materials, will not be able to reach. However, hybrid organic/inorganic materials are more likely to present new specificities that will meet the needs. In this context, the elaboration of new hybrid materials with fine control of their chemical composition and morphology by self-assembly, is critical to the development of next-generation materials.

Within the soft matter field, block copolymers (BCPs) is a very interesting class of materials due to their ability to self-assemble in different nano-phases dictated by the interaction between the two blocks but also easy and fast bottom-up processes. This specificity makes them promising candidates for emerging nanotechnologies such as nanotemplating[5], nanoporous membrane[6] or anti-reflection coating[7]. Meanwhile, the elaboration of copolymers based on a semi-conducting block has been developed in order to better control the nano-organization of conjugated polymers, especially for photovoltaics application[8]. Conjugated polymers are rigid molecules due to the (fused) aromatic rings making up the backbone of the chains. Three parameters influence the organization of a BCP; *f* the volume fraction of the blocks, χ the Flory-Huggins interaction parameter and N number of repetitive units.[9,10] Nevertheless, for rigid rod–coil copolymers, an additional component, μ the Maier-Saupe interaction parameter, needs to be taken into consideration.[11,12] Indeed, the π-π stacking occurring in the rod-phase will largely affect the organization of the macromolecules.[9,13] When the $\pi-\pi$ interactions are strong and $\mu > \chi$, the self-assembly will be dictated by the rod block and nano-fibrils will be formed instead of the typical lamellae, cylinders or spheres. Among the semi-conducting polymers, the Poly(3-hexylthiophene) (P3HT) based polymers are extensively studied for organic electronics applications. Many strategies are used to synthesize block copolymers from regioregular poly(3-hexylthiophene) to produce electronical materials with variable conductivities[14,15]. Poly(3-hexylthiophene) P3HT-based copolymers films are often composed of fibrils and long range order structuration is difficult to obtain, which is limiting their use for lithography[16–18].

To overcome the influence of $\pi-\pi$ stacking over the organization of P3HT based copolymer, different strategies have been followed. Lee *et al.* have synthesized several poly(3-hexyl thiophene-*b*-vinylpyridine) (P3HT-*b*-P2VP) copolymers to vary the size of the coil block. The authors proved by atomic force microscopy (AFM) and X-ray scattering that spherical and cylindrical phases could be obtained when the P2VP block was long enough[19,20]. On the contrary, Lin and coworkers played with the rod block chemical structure to decrease the π-π interaction.[21] They replaced the hexyl side chain of P3HT by longer or branched alkyl group to increase the bulkiness around the aromatic backbone of the chain and hinder crystallization. With this strategy the copolymer, with poly(methylmethacrylate) as the coil block, led to films with cylindrical domains. In a recent paper, our group also reported the formation of ordered structuration of an ionizable "clicked" P3HT-*b*-PMMA introducing a single cationic charge at the junction of the two blocks. X-ray scattering, DSC and AFM were used to reveal the decrease of the $\pi-\pi$ stacking together with the disappearance of the fibrils[22,23].

The incorporation of nanoparticles within block polymers BCPs has evolved into an area of considerable research[24–30], and comprehensive reviews are available[31–34]. These studies have established that the spatial distribution of the nanoparticles is sensitive to factors such as selectivity[35–37] and size[38–40]. For example, Chiu *et al.*[25] used surface modification of gold nanoparticles to drive their assembly when dispersed on symmetric coil-coil polystyrene-*block*-poly(2-vinylpyridine) PS-*b*-P2VP. PS-thiol coated gold nanoparticles are located near the center of the PS block phase of the lamellae structure, whereas P2VP-thiol coated gold nanoparticles were located in the P2VP domains. Particles coated with a specific polymer will lower their enthalpy by segregating into the corresponding domain of the block copolymer. When the same gold nanoparticles were grafted with a composite brush made of both PS and P2VP thiols they were found at the block interfaces in the resulting film. Yeh and coworkers showed the incorporation of acid-modified CdS nanoparticles NPs into the poly(4-vinylpyridine) P4VP block *via* hydrogen interaction in a PS-*b*-P4VP film[41]. Moreover, they proved the morphological transformation of the PS-*b*-P4VP self-assembly from the original *hexagonal-close-packed hcp* cylinders to lamellar structure when the NPs were added.

In the present work, we study the incorporation of functionalized gold nanoparticles (GNPs) into a diblock copolymer designed with a semi-conducting P3HT rod block and a coil

poly(ethylene glycol) methyl ether methacrylate PEGMA, which presents interesting properties for bio-applications[42–44]. Synthesis of the diblock copolymer and surface functionalization of NPs are thoroughly described. For the first time, the controlled localization of grafted GNPs was reported to influence the self-assembly of a rod-coil copolymer made up of a conjugated rod block and thus counteract the $\pi-\pi$ interactions. The impact of grafted GNPs on rod-coil diblock copolymer self-assembly and the film morphology changes were characterized by AFM, TEM, DSC and surface analysis techniques. X-ray Photoelectron Spectroscopy (XPS) was used to quantify gold nanoparticles at the surface of the hybrid film (HF) and Time-of-Flight Secondary Ion Mass Spectrometry (ToF-SIMS) allowed to precisely locate the functionalized gold nanoparticles inside the hybrid film.

Experimental section

Materials. All chemicals were purchased from Sigma Aldrich. CuBr was stirred with acetic acid during 16 hrs, washed with acetic acid, absolute ethanol, and finally diethyl ether to remove impurities. The commercial solution of 2,5-dibromo-3-hexyl thiophene in THF was stirred in a dried Schlenk and degazed for a few seconds to remove oxygen.

Characterization.

Diffusion order spectroscopy (DOSY) and ^{1}H NMR experiments were performed on a Bruker 400 MHz spectrometer in CDCl3 at 27 °C. All spectra were recorded on a Bruker AVANCE 400 MHz spectrometer. Chemical shifts are reported as ppm downfield from Tetramethyl silane (TMS).

Size exclusion chromatography (SEC) was carried out in THF with a flow rate of 1.0 mL.min^{-1}. One pre-column and two columns (Styragels HR 5E and 4E (7.8 ´ 300 mm)) were used for the analysis. Four detectors were combined; a UV-visible spectrophotometer (Viscotek VE 3210), Multi-Angle Light Scattering (Wyatt Heleos II), viscosimeter (Wyatt Viscostar II) and refractive index detector (Viscotek VE 3580). A Polystyrene calibration was used to calculate dispersities.

UV-Vis spectroscopy measurements were carried out in spectrum mode using a SHIMADZU UV-2450 spectrophotometer controlled by a software. The sample was solubilized before analysis in an appropriate solvent and inserted in a quartz cell having an optical path length of 1 cm.

Differential scanning calorimetry (DSC) was performed using a Q100 from TA instruments under N_2 atmosphere. For each sample, the temperature was increased from 40 to 240 °C with a ramp of 10 °C/min, then cooled to -65 °C at the same ramp. This was repeated during a second cycle.

XPS measurements were performed on a Thermo K-alpha spectrometer with a hemispherical analyzer and a microfocused (400 µm diameter microspot) monochromated radiation (Al Kα, 1486.6 eV) operating at 72 W under a residual pressure of 1.10^{-9} mbar. The pass energy was set to 20 eV. Charge effects, currently important for hybrid sample, were compensated by the use of a dual beam charge neutralization system (low energy electrons and Ar^+ ions) which had the unique ability to provide consistent charge compensation. All spectra were energy calibrated by using the hydrocarbon peak at a binding energy of 285.0 eV. Spectra were mathematically fitted with Casa XPS software© using a least squares algorithm and a nonlinear Shirley-type background. The fitting peaks of the experimental curves were defined by a combination of Gaussian (70%) and Lorentzian (30%) distributions. Quantification was performed on the basis of Scofield's relative sensitivity factors[45]

Time-of-Flight Secondary Ion Mass Spectrometry (ToF-SIMS) analyses were performed using a TRIFT V nanoToF II (Physical Electronics, US) equipped with a 30kV Au LMIG primary ion gun. All mass spectra were acquired in the positive polarity with the same experimental conditions, so that to perform semi-quantitative analysis (comparing the ratio of peaks intensities). For surface analysis, the LMIG gun was tuned to deliver Au_3^{++} gold clusters primary ions with a DC current of 7 nA over a 10 µm raster size, the mass range was fixed between 0 and 1850 uma and the number of frames was set to 50 (dose: $3.7x10^{11}$ions/cm^2). Depth profile experiments (series of 20 cycles "analysis/sputtering") were carried out using Au_3^{++} primary ions over 10x10µm^2 raster size for analysis and a 1 kV Ar^+ gas gun for etching (with a sputtering time of 20 seconds for each cycle, a DC current of 50 nA and a sputtered area of 100x100 µm^2). For 2D imaging, a resolution of 512x512 pixels with a time per channel of 256, over 100x100 µm^2 raster size was used. Note that dual charge (e^-/Ar^+) compensation was used for all analyses and the sodium peak, which appears with a high intensity, has been blanked during the experiments so that to detect better smaller peaks. Data processing was performed using ToF-DR software provided by Physical Electronics. All positive polarity mass spectra were calibrated using CH^+(m/z 13), CH_2^+ (m.z 14) and C_2H^+ (m/z 25) peaks.

Atomic force microscopic (AFM) was carried out on a MultiMode® 8 Atomic Force Microscope (AFM) from Bruker in the PeakForce Quantitative NanoMechanics mode.

Transmission Electron Microscopy images of gold nanoparticles were performed on a Philips CM 200 (200 kV) TEM microscope equipped with a LaB6 source. The particles dispersed in water or chloroform were dropped onto a carbon-coated copper grid and dried before analysis.

Transmission Electron Microscopy pictures of hybrid films were performed on a Talos F200S G2 Thermofisher – Eindhoven -Transmission Electron Microscope at 200kV, equipped with a Camera ONE VIEW – Gatan – Paris for image acquisition. Before observation, the films were dip-coated on Thermanox substrates and cross cut using a Cryo-ultramicrotome UC-7 FC7 – Leica Microsystems. The use of this substrate allows the elaboration of thin cross-section slices using an ultramicrotome. TEM images have been performed after film treatment with ruthenium tetraoxide to enhance electronic contrast. This chemical reacts with thiophene moities, colors the P3HT domains (dark zones) and thus increases the contrast with PEGMA environments (clear areas). Cross sections were performed at -90°C using a Cryo-knife 35°. Polymer's samples were contrasted with Ruthenium Tetraoxide aqueous solution (0.5%).

Synthesis

Synthesis of ethynyl-terminated P3HT. P3HT was synthesized according to the procedure described in a previous work.[46] In a dried Schlenk flask, 2,5-dibromo-3-hexyl thiophene (6.13 mmol) was degazed under vacuum for 3 seconds. Then 10 mL of dried THF were introduced as the solvent. Isopropyl magnesium chloride (6.13 mmol) was added and the media was stirred for two hours at 20°C under nitrogen atmosphere. Dried THF (40 mL) containing Ni(dppp)Cl_2 (0.34 mmol) was then added to the solution and reacted during ten min.

Eventually, of ethynyl magnesium chloride (1.84 mmol) was inserted in the media for an additional 2 min. The mixture was precipitated twice in methanol and the obtained polymer was characterized by SEC (M_n = 6 500 g mol^{-1}; $Đ$ = 1.3) and ^{1}H NMR (400 MHz, $CDCl_3$): δ = 0.91 (*t*, 3 H), 1.34 (*m*, 6 H), 1.69 (*t*, 2 H), 2.80 (*t*, 2 H), 3.53 (*s*, 1 H), 6.97 (*s*, 1 H).

Synthesis of azido functionalized PEGMA (PEGMA-N_3). P(EGMA-*stat*-MEO_2MA) was prepared by Atom Transfer Radical Polymerization initiated by 2-azidoethyl 2-bromoisobutyrate. Copper bromide (26 mg, 0.18 mmol) and *N,N,N′,N″,N″*-PentaMethylDiEthyleneTriAmine (PMDETA) (62.4 mg, 0.36 mmol) were added to a Schlenk

flask sealed with a septum. Next, a degassed mixture of both monomers oligo (ethylene glycol) methacrylate (0.9 g, 1.8 mmol) and 2-(2-methoxyethoxy)ethyl methacrylate (3 g, 16.2 mmol) and 3 mL of dioxane were added through the septum with a degassed syringe. The flask was put in an ice bath and purged with nitrogen for 30 minutes. Then the initiator, 2-azidoethyl 2-bromoisobutyrate (14.1 mg, 0.06 mmol) was added with a microliter syringe. The mixture was heated at 75 °C in an oil bath and stopped 30 minutes later. The experiment was stopped by opening the flask to expose the catalyst to air. Dialysis was used to remove free monomers and purify the azido-terminated PEGMA-N_3. The mixture was diluted with ethanol and dialyzed with deionized water using a regenerated cellulose membrane RC (weight cut off: 3.5 kDa) for one week. Water was removed by putting the polymer solution in a crystallizer glass to let water evaporate itself at room temperature for 3 days. The pure polymer appeared as a colorless viscous oil. The polymer was characterized by NMR, and SEC (M_n=18 000 g.mol^{-1}; $Đ$ = 1.2) after drying it under vacuum. ^{1}H NMR (400 MHz, $CDCl_3$): δ ppm = 0.83 (*s*, 3 H), 1.81 (*m*, 2 H), 3.46 (*t*, 2 H), 3.59 (*m*, 3 H), 3.76 (*m*, 3 H), 4.11 (*m*, 2 H).

Synthesis of P3HT-b-PEGMA copolymer (Scheme S1)**.** P3HT (1 eq), PEGMA-N_3 (1.2 eq) and CuBr (10 eq) were dissolved in THF (40 mL) and submitted to three freeze-vacuum cycle to remove oxygen. PMDETA (10 eq) was then added and the media was stirred at 50 ºC for 2 days. The solution was then purified through a basic alumina column to remove copper bromide precipitated in methanol. The obtained polymer was washed by Soxhlet extraction with methanol, cyclohexane, and chloroform. Acetone and cyclohexane washing were performed to remove residual homo PEGMA and homo P3HT respectively.

Synthesis of gold nanoparticles and functionalization with PEG-thiol ligand. Small citrate-capped gold nanoparticles were first synthesized according to the protocol reported by Jana and Murphy[47] to obtain small gold nanoparticles (3-5 nm). Briefly, $HAuCl_4$ and trisodium citrate were solubilized in 20 mL of deionized water at a concentration of 2.5 mM for both reagents. 0.6 mL of a 0.1M $NaBH_4$ solution was then added at once in the gold solution under a constant and strong stirring. The solution turned from yellow to a wine-red color. After 15 minutes stirring, 2.5 mM of PEG_{800}-SH was added and the reaction was left for 4 hours to complete the exchange of ligands, stopped and dialyzed against deionized water using a regenerated cellulose membrane RC (weight cutoff: 8 kDa) for 3 days (Scheme SI2).

Film preparation

The hybrid films were prepared through a dip-coating process. Silicon wafers or Thermanox® substrates were vertically withdrawn at 10 µm/s from a 1 mL chloroform suspension of gold nanoparticles containing 3 mg of $P3HT_{6.5}$-*b*-$PEGMA_{18}$. The concentration of the gold suspension in chloroform was set so that the hybrid film will contain 0, 2, 5 or 10 vol%.

Results and Discussion

Synthesis of the diblock copolymer P3HT-b-PEGMA. A P3HT-*b*-PEGMA block copolymer was synthesized in 3 steps, ATRP of a mixture of MEO_2MA and OEGMA monomers using 2-azidoethyl-2-bromoisobutyrate as an initiator, GRIM polymerization of 3-hexylthiophene and the click reaction of both homopolymers. The purification of the ethynyl-terminated P3HT was performed as described previously in the experimental section to avoid the denaturation of the alkyne end-chain. Using the integration of the methylene proton at 2.8 ppm by ^{1}H NMR, a P3HT degree of polymerization of 35 units was estimated (Figure S1). This value was in agreement with the molecular mass determined by SEC (M_n = 6 500 g.mol^{-1}). The alkyne end-chain functionalization was calculated to be efficient at 92% by integration of the signal at 3.5 ppm.

The azido end-capped PEGMA was synthesized using 2-azidoethyl-2-bromoisobutyrate as initiator to introduce an azide moiety at the end of the chains from the initiator avoiding post-modification.[48] Due to the high molecular weight of the synthesized PEGMA-N_3, we were not able to calculate the degree of polymerization by ^{1}H NMR since the CH_2 in alpha or beta position of the azide group has the same chemical shift with the repeat units; the methylene group in alpha position of the methacrylate (4.15 ppm) (Figure S2). The molecular weight determined by SEC using PS standard is M_n = 18 000 g.mol^{-1}. The ratio of the integration values of the CH_2 in *alpha* position of the methacrylate group with the other CH_2 is 1.0 : 4.3 for a theoretical value of 1.0 : 4.4. The final composition of the thermo-responsive homopolymer is then 90 and 10% of MEO_2MA and OEGMA, respectively.

P3HT-*b*-PEGMA was prepared using a click reaction between the ethynyl-P3HT and the azido-terminated PEGMA as described in Scheme SI1. Since it is easier to remove free PEGMA than to remove free P3HT due to versatile solubility, an excess of PEGMA-N_3 was used to perform the click reaction with the ethynyl-P3HT.[48] Since P3HT shows a maximum light absorption at 460 nm, we were able to control and monitor the cyclo-addition reaction *via* SEC using UV-

visible detector (Figure S3). A shift of the molecular weight was observed compared to the homo P3HT, showing an increase of the diblock copolymer molecular weight (Figure S4). A single and narrow peak was observed with a dispersity value $Đ$ of 1.2, confirming the successful purification of the diblock copolymer. The Diffusion Ordered SpectroscopY (DOSY) NMR analysis of the P3HT-*b*-PEGMA also confirmed the success of the click reaction since all ^{1}H signals belonged to the same macromolecule (Figure 1).

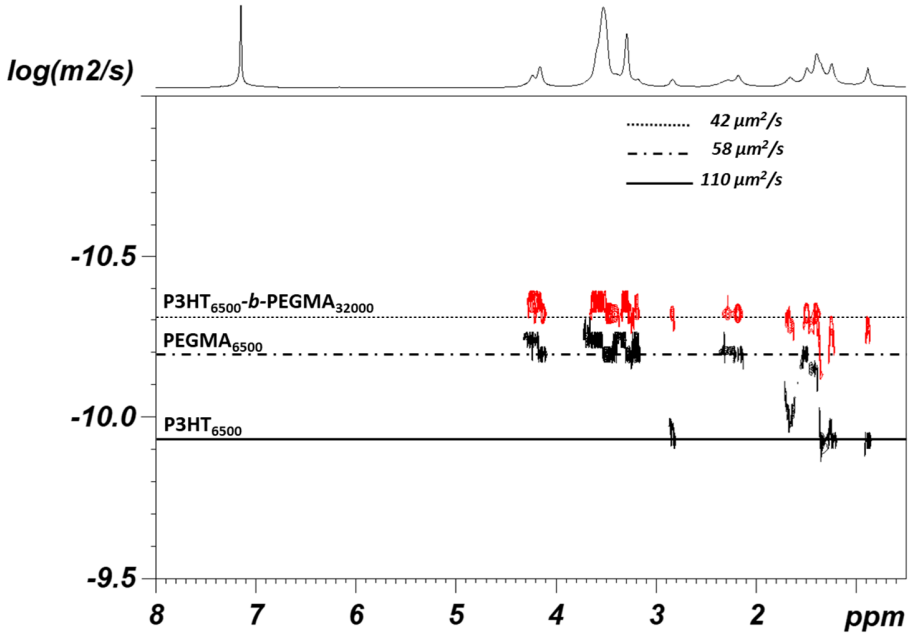

Figure 1. DOSY NMR of the P3HT-*b*-PEGMA copolymer and its building blocks.

The two parent homopolymers ethynyl-P3HT and PEGMA-N_3 showed higher diffusion coefficients values than the one from the diblock copolymer. The ethynyl-P3HT with the smallest molecular weight of 6 500 g.mol^{-1} showed the highest diffusion coefficient value around 110 µm^2/s in comparison with the lowest diffusion coefficient value of 42 µm^2/s for the final P3HT-*b*-PEGMA (M_n = 24 500 g.mol^{-1}).

The integration of the area under the ^{1}H NMR peak at 2.8 ppm corresponding to the methylene protons of the thiophene and the methylene units in *alpha* position of the methacrylate group, allowed to calculate a molar composition P3HT/PEGMA of 1/2 (Figure S5). Since DP_n of the

P3HT block was equal to 35, the PEGMA block had a DP_n of 70, which was consistent with a molecular weight of 18 000 g.mol^{-1} (Table 1).

Table 1. Summary of the polymers' characteristics.

Polymer	M_n [a] (g.mol^{-1})	DP_n [a]	M_n [b] (g.mol^{-1})	$Đ$ [b]	f [c] P3HT
Ethynyl-P3HT	6 000	35	6 500	1.31	1
PEGMA-N_3	--	72	18 000	1.20	0
P3HT-*b*-PEGMA	22 000	--	24 000	1.20	0.33
PEG-SH *NP ligand*	750	17	800	1.1	--

[a] calculated by ^{1}H NMR [b] Calculated from SEC via PS calibration. [c] The P3HT volume fraction was calculated by using M_n provided by ^{1}H NMR and the polymer densities: ρ_{P3HT} = 1.11 g/mL and ρ_{PEGMA} = 1.19 g/mL

Synthesis and characterization of gold nanoparticles.

UV-Vis analyses in water of both of citrate and PEG-thiol capped nanoparticles show a red-shift of the gold nanoparticles absorption from 515 nm to 530 nm (Figure 2a) after functionalization. This confirms the ligand exchange during the functionalization step where citrate was replaced by the PEG-thiol (Scheme SI2).

TEM image of gold nanoparticles after functionalization by the PEG-thiol ligand is shown in Figure 2b. The TEM photo exhibits spherical NPs with an average diameter around 5 nm without aggregation indicating their efficient stabilization by PEG corona.

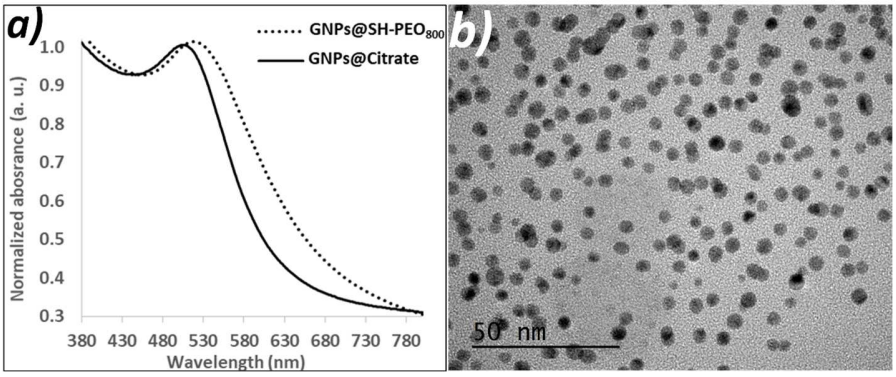

Figure 2. UV spectra of gold nanoparticles before and after ligands exchange with PEO (a) and TEM micrograph of the synthesized PEO_{800}-capped gold nanoparticles (b).

XPS surface analyses of the nanoparticles confirm these previous UV-Vis observations. C1s spectrum of citrate-capped gold nanoparticles is depicted in Figure 3a. Three components are clearly observable at 285, 286.5 and 288.8 eV corresponding to C−C, C−OH and COO bonds, respectively.[49,50] The C−C and C−OH components can be attributed to alkyl and alcohol groups in citrate. On the other hand, the COO component is attributed to the carboxylate function of citrate. The intensity ratio between COO and C−OH was calculated to be 3.3, close to 3 as it is in the composition of citrate ($^{-}$OOC−CH_2−C(OH)COO^{-}−CH_2−COO^{-}). The O1s spectrum of citrate-capped gold nanoparticles has been fitted in two peaks (Figure 3b). The first peak at 531.7 eV was attributed to the oxygen atoms in COO environment and the one at 536 eV to the oxygen atom of the alcohol group[50–53]. The atomic ratio of oxygen between the carboxylate group and the alcohol was equal to 5.9, in agreement with the citrate formula (6.0).

The C1s spectrum of PEG-thiol-capped gold nanoparticles was similar to the C1s spectrum of the commercial PEG-thiol used for the functionalization of gold nanoparticles, only two components at 285 and 286.5 eV are observed (Figure 3c). Indeed, the contribution of carboxylate environment at higher energy (288.8 eV) has disappeared indicating the replacement of citrate ligand by PEG-thiol. In addition, the contribution at 286.5 eV can be attributed to the C−O bond from the PEG ligand and C−S bond linked to the surface of gold. The latter cannot be discriminate from the former. The component at 285 eV is from the C−C bonds. The O1s spectrum of PEG-capped nanoparticles showed only one component at 532.7 eV (Figure 3d). This is typical of the C−O environment in PEG. Most importantly, the oxygen contribution at higher energy (536 eV) from the alcohol in citrate-capped nanoparticles has completely disappeared, indicating that the citrate ligand is no longer present.

Note that for all spectra, the C1s component located at 285 eV is attributed to the C−C bonds of the molecules probed but also to adventitious carbon (C−C and C−H species), always present at the surface analyzed by XPS.

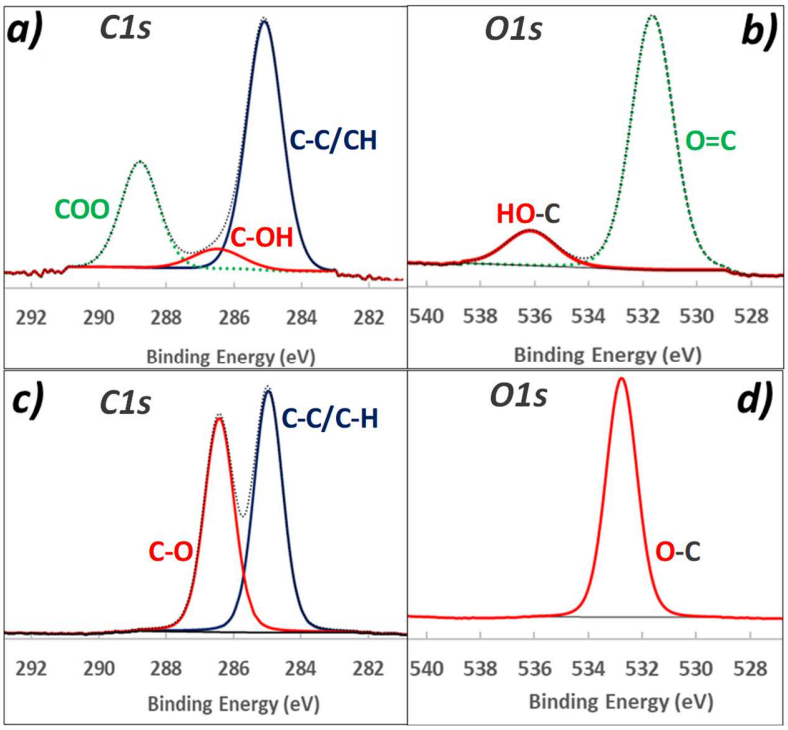

Figure 3. C1s XPS spectra of citrate-capped GNPs (a) and PEG_{800}-capped GNPs (c). b) and d) are O1s spectra of citrate-capped GNPs and PEG_{800}-capped GNPs respectively.

Diblock copolymer Self-assembly. Thin films of the diblock copolymer, *i.e.* without gold nanoparticles, were dip-coated from a chloroform solution at 3 $g.L^{-1}$ onto silicon wafer. The thickness of the films was evaluated to be around 200 nm by the TEM observation of the film cross section. AFM images of the top surface of the films and XPS analysis are shown in Figure 4. The deconvolution of C1s spectrum of P3HT-*b*-PEGMA film without any amount of gold nanoparticles shows 4 components (Figure 4 a). The first peak at 285 eV is from the C–C bonds from both P3HT and PEGMA homopolymers. The second peak at 286.7 eV is related to the C-O bonds in the PEGMA bloc and the C–S bonds from P3HT. The small intensity peak at 287.7 eV is due to the π-π* shake-up transition in the thiophene cycle[54]. The peak at higher energy can be attributed to the COO bond from the methacrylate group.

The height and adhesion images show a random organization of nanofibrils of 10 nm in width and several hundred nanometers in length (Figure 4 b-c). This morphology is typical of rod-coil diblock copolymer when the rod block crystallization dominates over the block

copolymer self-assembly.[19] Phase diagram of coil- coil BCPs with equivalent composition, *i.e.* $f_{vP3HT} = 0.33$ for a P3HT$_{6.5k}$-*b*-PEGMA$_{18k}$ would normally lead to a structure of P3HT cylinders in a PEGMA matrix.[55] In that case, BCPs self-assembly is governed by the volume fraction *f* of the blocks and the χN product.[9] For the P3HT$_{6.5k}$-*b*-PEGMA$_{18k}$ the rigidity and the π-π interactions coming from the P3HT aromatic structures control the macromolecular interactions, which are dominated by the strong rod regime where $\mu > \chi$.

PEG-decorated gold nanoparticles GNP@PEG were then added at 2, 3, 5 and 10 vol % to the copolymer solution and films were dip-coated onto silicon wafer. AFM images and XPS of the hybrid films are depicted in Figure 4. C1s spectra of the hybrid films obtained after the incorporation of PEG-thiol-capped gold nanoparticles show an increase of the intensity of the peak at 286.7 eV with the amount GNP@PEG added. When the amount of GNP@PEG incorporated inside the film was increased (2 v%, 5 v% and 10 v%), the intensity of the C-O component increased as well (Figure 4 d, 4g and 4j). This is increase of the intensity of the C-O peak is due to the fact that the incorporated gold nanoparticles are PEG-capped and the C-O bond from –(CH_2–CH_2–O)– PEG units appears at 286.5 eV[56]. A slight decrease of the intensity of the COO peak from the methacrylate (289 eV) was observed. This is probably due to the diminution of its ratio as the global concentration of carbon increases with the amount of PEG-capped nanoparticles added.

Both height and adhesion images showed that fibrils organization gradually disappeared with the increase of the gold nanoparticles. Indeed, for the lowest volume fraction, P3HT fibrils were observed in the top surface of the thin film (Figure 4 d-f). Then for 5 vol% of GNP@PEG, the surface is equally partitioned in both nano-domains in a PEGMA matrix with the remaining presence of fibrils and new *out-of-the-plane* P3HT cylinders-like (Figure 4 g-i). With the introduction of 10 vol % of GNP@PEG, the fibrils are almost completely erased and the *out-of-the-plane* cylindrical-like morphology is observed on the whole surface (Figure 4 j-l).

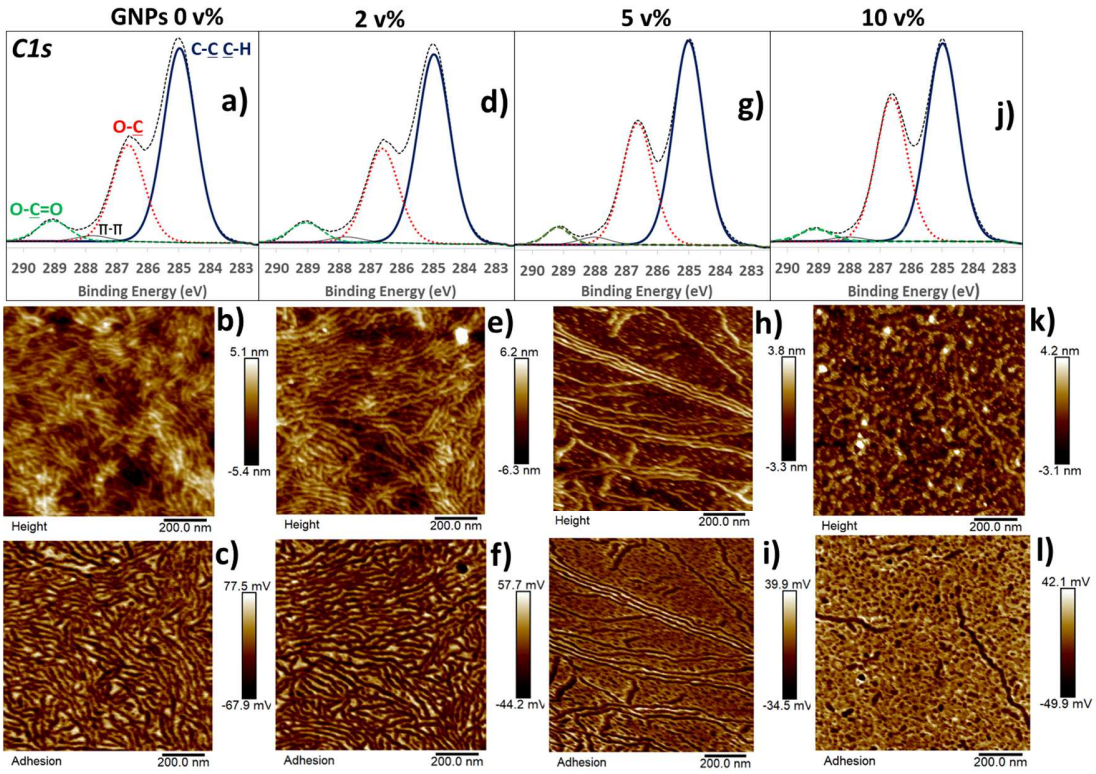

Figure 4. C*1s* XPS spectra of the hybrid films with a volume fraction of 0%, 2%, 5% and 10% in gold nanoparticles for a), d), g) and j), respectively. PeakForce QNM-mode AFM images of the hybrid films with a volume fraction of 0%, 2%, 5% and 10% in gold nanoparticles b-c), e-f), h-i) and k-l), respectively.

The spatial distribution of the incorporated GNPs inside the hybrid film was then investigated by ToF-SIMS (Figure 5). First of all, pure films based P3HT or PEGMA homopolymers, P3HT-*b*-PEGMA copolymer or GNPs@PEG were separately analyzed in order to establish a database with the main specific peaks of each species (Table 2).

Table 2. Main secondary ions detected by ToF-SIMS for P3HT, PEGMA, P3HT-*b*-PEGMA, GNPs@PEG and P3HT-*b*-PEGMA + GNPs@PEG films over a 0-200 mass range in the positive polarity.

Samples	m/z	Ions
PEGMA	71	$C_4H_7O^+$
	139	$C_7H_7O_3^+$
	141	$C_7H_9O_3^+$
P3HT	81	C_4HS^+
	117	$C_6H_{13}S^+$
	147	$C_9H_7S^+$
GNPs@PEG	45	$C_2H_5O^+$
	197	Au^+
P3HT-*b*-PEGMA	81	C_4HS^+
	115	$C_6H_{11}S^+$
	139	$C_7H_7O_3^+$
	141	$C_7H_9O_3^+$
P3HT-*b*-PEGMA	45	$C_2H_5O^+$
+ GNPs@PEG	81	C_4HS^+
	139	$C_7H_7O_3^+$
	141	$C_7H_9O_3^+$
	197	Au^+

Figure 5a presents the positive ion mass spectra of P3HT-*b*-PEGMA + 10 vol% GNPs@PEG hybrid film over m/z 50-250 (top spectrum) and m/z 280-440 (bottom spectrum) mass ranges. Characteristic peaks of the PEGMA methacrylate polymer backbone [57,58] homopolymer are detected at m/z =139 ($C_7H_7O_3^+$), 141 ($C_7H_9O_3^+$) and 143 ($C_7H_{11}O_3^+$), as well as a fragment characteristic of the sulfur containing ring of P3HT block at m/z = 81 (C_4HS^+), and the Au^+ peak at m/z=197 specific of GNPs. Moreover, polymer structure patterns, composed of a main peak surrounded by smaller peaks resulting of the loss or the gain of 2 protons, are also detected at bigger masses: from m/z = 313 to m/z =319, from m/z = 371 to m/z =377 or from m/z = 429 to m/z =435 (Figure 5a bottom spectrum). Note that the fragmentation patterns of the two homopolymers appear to be slightly different after their incorporation in the block copolymer macromolecular structure with and without GNPs (see Table 2). For example, for the P3HT homopolymer, the positive ion peaks at m/z=147 and m/z=149 attributed to $C_9H_7S^+$ and $C_9H_9S^+$ respectively are not detected anymore for the block copolymer. The 2D chemical mapping of $C_7H_7O_3^+$ ions (characteristics of the copolymer, in green) and Au^+ ions (characteristics of GNPs, in red) over a 100x100µm field of view in positive polarity (Figure 5b) shows a homogeneous distribution of GNPs at the surface of the hybrid film. Moreover, richer areas of the copolymer

fragment (in bright green) are distinguishable, maybe due to topography effects. In order to obtain information about the GNPs spatial distribution more deeply in the copolymer bulk material, ToF-SIMS depth profile experiments (series of 20 cycles "analysis/sputtering") were performed on the hybrid film containing 10 vol% of GNPs. Figure 5c presents the concentration depth profiles of $C_7H_7O_3^+$ (representing the copolymer, in green), Au^+ (specific to GNPs, in yellow) and total secondary ions detected (in blue) obtained in the positive polarity over 380 seconds of etching. Concerning $C_7H_7O_3^+$ and Au^+ profiles, they remain constant from 25s to the end of the sputtering. A 3D image has been reconstructed from the depth-profiles where the signal intensities of $C_7H_7O_3^+$ (in green) and Au^+ (in yellow) are plotted over the analyzed area (10µmx10µm = x and y dimensions) versus the etching time (the z axis, 280s); for a better visibility, the z axis is over-dimensioned compared to the other two axes. Note that it is difficult to determine precisely the sputtered depth due to the unknown sputtering ion yield of the hybrid organic-inorganic material. However, it is reasonable to say that only few tens of nanometers have been removed, regarding the very smooth etching conditions used (1kV, 50nA). The 3D image clearly shows that the spatial distribution of GNPs follows the one of the copolymer in the analyzed volume. The two species are well connected and they are homogenously present in the bulk of the material due the strong interaction of the GNPs@PEG with the PEGMA domains. This ToF-SIMS study confirms that the self-assembly of the hybrid film occurs without any macro segregation between the gold functionalized GNPs and the diblock copolymer.

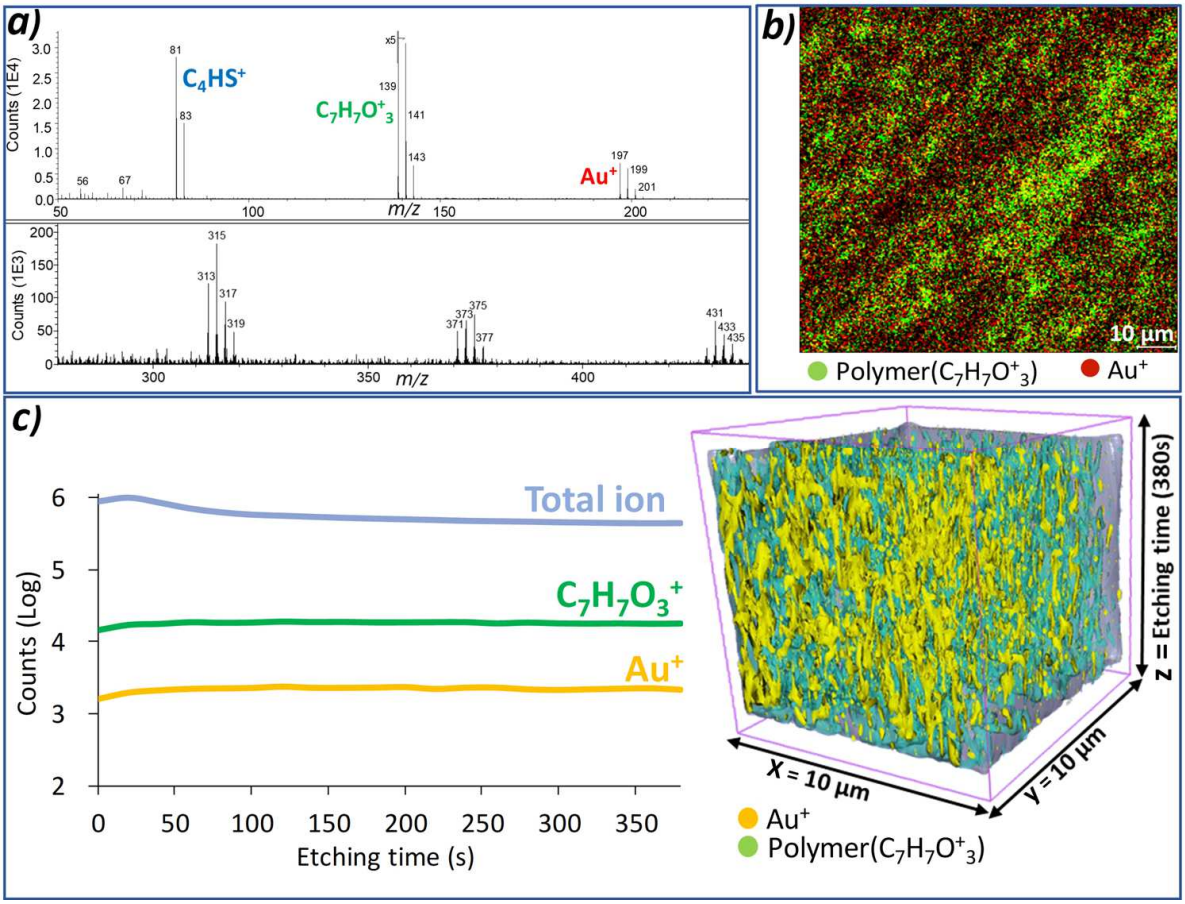

Figure 5. a) TOF-SIMS positive ion mass spectra of P3HT-*b*-PEGMA + GNPs (10 v%) hybrid film over m/z 50-250 (top spectrum) and m/z 280-440 (bottom spectrum) mass ranges, b) TOF-SIMS 2D chemical mapping of $C_7H_7O_3^+$ and Au^+ ions over a 100x100µm field of view in positive polarity c) TOF-SIMS depth-profile experiment over 380s etching time of $C_7H_7O_3^+$ (green) and Au^+ (yellow) ions in positive polarity and 3D image reconstruction from the depth-profile showing the spatial distribution over 10x10µm^2 raster size and 380s etching time of $C_7H_7O_3^+$ (green) and Au^+ (yellow) ions at the surface of P3HT-*b*-PEGMA + GNPs (10 v%) hybrid film. For a better visibility, the z axis is over-dimensioned compared to the other axes.

The role of GNPs in the structural modification from fibrils to cylinder like morphology was then investigated. First, TEM experiment was performed on cross-section transversal slices of hybrid films dip-coated on a polymer substrate (Thermanox®) to study the location of the GNPs within the films. TEM images of the hybrid film showed a clear segregation between the two polymer areas, pictured by light and dark grey domains corresponding to PEGMA and P3HT domains, respectively (Figure 6a).

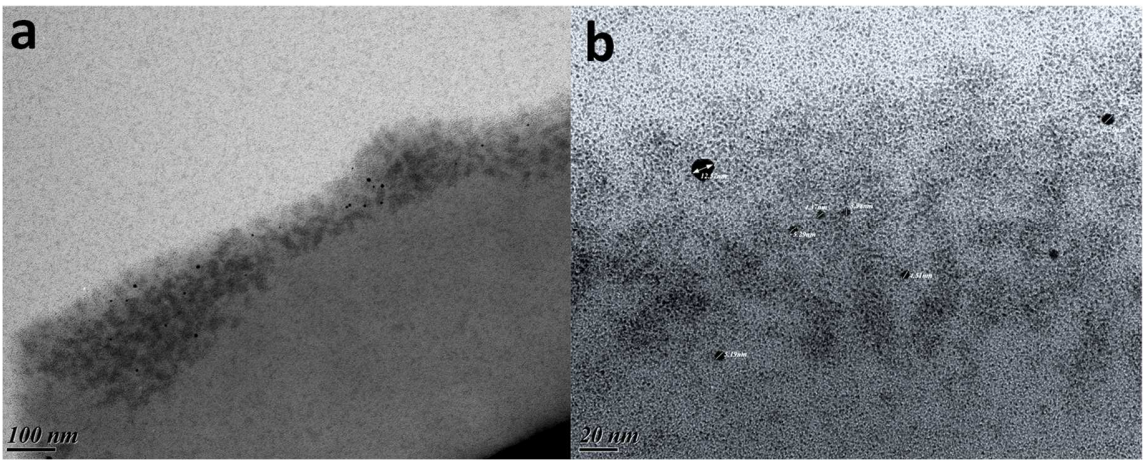

Figure 6. (a) TEM micrographs of a cross section the diblock copolymer-GNP@PEG (5 vol%) hybrid film contrasted with ruthenium oxide RuO_4 for 90 min. (b) is the magnification picture of (a).

As it can be clearly observed on the high magnification picture (Figure 6b), GNPs (black spots) are preferentially localized in the light grey PEGMA domains, due to their functionalization with PEG ligand and their hydrophilic affinity. Additional image where GNPs are clearly visible inside the block copolymer film is available in supporting information (SI7). As a consequence of the GNP@PEG insertion in the PEGMA block, the volume fraction of the corresponding phase increases and then influences the diblock copolymer self-assembly. In the literature, other strategies were followed to reduce the predominance of $\pi-\pi$ interactions over the morphology of P3HT-based copolymer films. Lee *et al.*[19] perfomed the synthesis of various P3HT-*b*-P2VP copolymers in which the P2VP degree of polymerization was changed. Fibrils were obtained for coil block fraction under 68 vol%. When the coil fraction was further increased, cylindrical and spherical phases were observed by AFM. The authors attributed such a variation to the chain twist generated for the bulkiness of the coil block which impeded π-π stacking. Herein, the copolymer has P3HT and PEGMA volume fraction of 0.33 and 0.67 respectively. After the addition of 10 vol% of GNP@PEG, the resulting P3HT volume fraction dropped at a maximum of 0.3. Although the difference in the P3HT content seems low, it is high enough to break the fibrils diblock copolymer self-assembly. To follow this trend, we investigated the morphology of a P3HT-*b*-PEGMA/PEGMA homopolymer blend with a volume ratio of 90/10 to reach a P3HT volume fraction of 0.3. AFM images show that the surface is composed of randomly aligned nano-fibrils without neither *in-the-plane* nor *out-the-plane*

cylindrical morphologies (Figure S6). It is worth noting that we observed an increase of the volume fraction of the PEGMA matrix, in which P3HT fibrils appeared more diluted.

Therefore, the increase in the volume fraction is not the only factor leading to the morphology transformation. Indeed the rigidity caused by the incorporation of hard metallic nanoparticles in the PEGMA phase could also impede the creation of $\pi-\pi$ stacking and therefore the crystallization of the P3HT. DSC of the composite blend (90/10 copolymer/particle in volume) was performed and compared to the pure diblock copolymer and to the parent P3HT homopolymer to check the influence of the NPs addition on the P3HT block crystallization. P3HT exhibited an endothermic peak at 210 °C corresponding to P3HT crystals melting temperature T_m (Figure 7a). This value is almost the same in P3HT-*b*-PEGMA thermogram, *i.e.* T_m = 220 °C, but with a weaker intensity due to the decrease of P3HT content and a possible decrease of the crystallization rate. Since PEGMA glass transition temperature is below -50°C, the crystallization of P3HT blocks is more affected by the size of the PEGMA block than by its rigidity. The heating scan of the blend containing gold nanoparticles present a lower endothermic peak at 195 °C with a weak intensity. This behavior may mean a significant reduction in the crystallinity of P3HT leading to the cylindrical microstructures observed by AFM.

In the cooling ramp, a similar trend was observed in the crystallization temperature T_c of the P3HT, P3HT-*b*-PEGMA and the hybrid blend, at 160, 125 and 95 °C respectively. This behavior indicates that the crystallization of the P3HT moieties is hindered by the addition of, first a large volume fraction of soft PEGMA, and then a small addition of hard nanoparticles. This kind of behavior has already been described by Dai *et al.*[59] when they studied the transition temperatures of different P3HT-*b*-P2VP with several coil block lengths. Indeed, the melting temperature Tc decreases from 200°C to 140°C with the decrease of the volume fraction of the P2VP block from 0.29 to 0.57. Above a volume fraction of 0.57 in the coil polymer, no crystallization was observed.

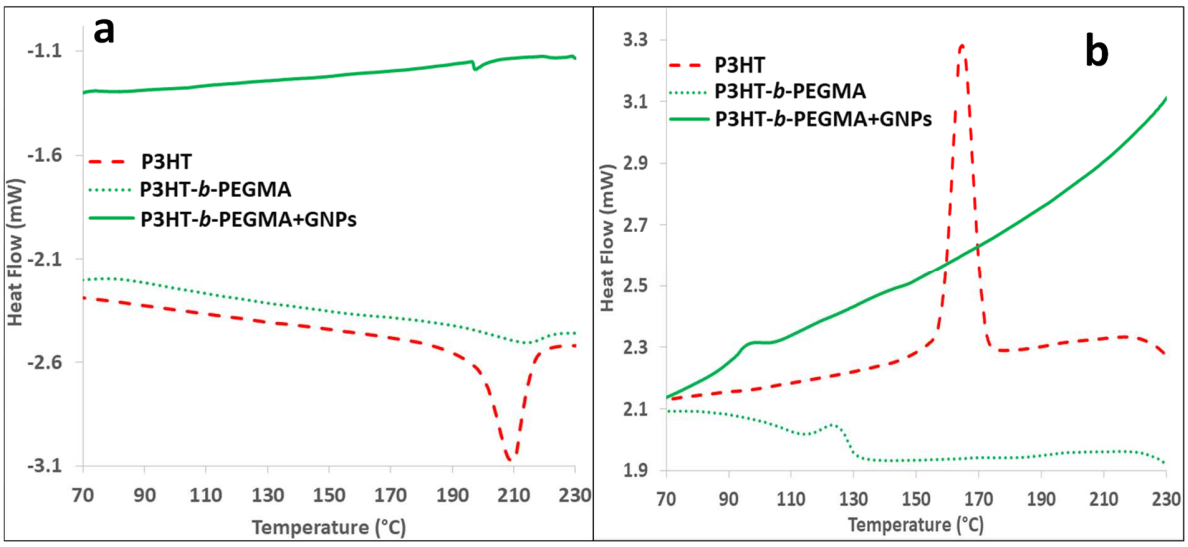

Figure 7. Thermogramms of the heating a) and the cooling of P3HT, P3HT-*b*-PEGMA and the hybrid film with 10 v % in gold nanoparticles b).

Thus, a morphological transition from P3HT fibrils into *out-of-the-plane* cylinders-like can be driven by introducing GNP@PEG during the nanophase segregation of the P3HT-*b*-PEGMA by self-assembly.

Conclusion

Herein is described the change of a diblock rod-coil copolymer film morphology driven by the addition of metallic nanoparticles NPs. The precise location of a small amount of gold NPS in the coil phase hindered the crystallization of the rod block. AFM images of the diblock copolymer shows the transition from a random organization of P3HT nanofibrils, as a typical organization of rod-coil block copolymers, where the crystallization of the rod block takes over the block copolymer self-assembly. From such a behavior, *out-of-the-plane* rod polymer cylinders-like in a coil polymer matrix are then observed. TEM of film cross sections shows the GNP@PEG embedded in the PEGMA regions thanks to the physical affinity brought by their surface functionalization with PEG chain corona. DSC revealed that the thermal transitions pertaining to the P3HT rod crystals disappeared after the addition of the GNPs. Such a morphological change triggers by the elaboration of a hybrid composite is of great interest for many applications. In this specific case, the use of a thermosensitive block PEGMA in which lower critical solubility temperature was tuned to be 37°C (Figure S8) by the introduction of a precise ratio of both OE_2MA and OEGMA monomers, [60,61] can allow very interesting biological

applications in the field of cellular culture and bioelectronic especially.[62–64] Further applicative works are in progress with these films using the light absorbing properties of both P3HT and GNPs into a thermosensitive biocompatible PEGMA matrix.

Supporting Information.

The supporting information provides synthetic scheme and chemical characterization (SEC, NMR) of the materials used in this study. Moreover, additional microscopy images can be found in the file.

AUTHOR INFORMATION

Corresponding Authors

e-mail: herve.martinez@univ-pau.fr; laurent.billon@univ-pau.fr;

Funding Sources

ACKNOWLEDGMENT

TEM Imaging of the hybrid film was performed at the Bordeaux Imaging Center, member of the FranceBioImaging national infrastructure (ANR-10-INBS-04). We thank S. Lacomme for her work on this project. Dr. A. Khoukh and J.B. Ledeuil are acknowledged for fruitful discussion on NMR and XPS analysis. We thank F. Portail, C. Bessibes, and F. Casbas of Arkema Industry for the TEM analysis realized on PEO-capped gold nanoparticles.

REFERENCES

(1) Huynh, W. U.; Dittmer, J. J.; Alivisatos, A. P. Hybrid Nanorod-Polymer Solar Cells. *Science* **2002**, *295* (5564), 2425–2427.

(2) Rosa, C. D.; Auriemma, F.; Girolamo, R. D.; Pepe, G. P.; Napolitano, T.; Scaldaferri, R. Enabling Strategies in Organic Electronics Using Ordered Block Copolymer Nanostructures. *Adv. Mater.* **2010**, *22* (47), 5414–5419.

(3) Ball, P. High-Density Memory: A Switch in Time. *Nature* **2007**, *445* (7126), 362–363.

(4) Lopes, W. A.; Jaeger, H. M. Hierarchical Self-Assembly of Metal Nanostructures on Diblock Copolymer Scaffolds. *Nature* **2001**, *414* (6865), 735–738.
(5) Ruiz, R.; Kang, H.; Detcheverry, F. A.; Dobisz, E.; Kercher, D. S.; Albrecht, T. R.; de Pablo, J. J.; Nealey, P. F. Density Multiplication and Improved Lithography by Directed Block Copolymer Assembly. *Science* **2008**, *321* (5891), 936–939.
(6) Phillip, W. A.; O'Neill, B.; Rodwogin, M.; Hillmyer, M. A.; Cussler, E. L. Self-Assembled Block Copolymer Thin Films as Water Filtration Membranes. *ACS Appl. Mater. Interfaces* **2010**, *2* (3), 847–853.
(7) Joo, W.; Park, M. S.; Kim, J. K. Block Copolymer Film with Sponge-like Nanoporous Strucutre for Antireflection Coating. *Langmuir ACS J. Surf. Colloids* **2006**, *22* (19), 7960–7963.
(8) Cuendias, A. de; Hiorns, R. C.; Cloutet, E.; Vignau, L.; Cramail, H. Conjugated Rod–Coil Block Copolymers and Optoelectronic Applications. *Polym. Int.* **2010**, *59* (11), 1452–1476.
(9) Olsen, B. D.; Segalman, R. A. Nonlamellar Phases in Asymmetric Rod−Coil Block Copolymers at Increased Segregation Strengths. *Macromolecules* **2007**, *40* (19), 6922–6929.
(10) Qian, L.; Yang, J.; Zhou, R.; Tang, A.; Zheng, Y.; Tseng, T. K.; Bera, D.; Xue, J.; Holloway, P. H. Hybrid Polymer-CdSe Solar Cells with a ZnO Nanoparticle Buffer Layer for Improved Efficiency and Lifetime. *J. Mater. Chem.* **2011**, *21* (11), 3814–3817.
(11) Holyst, R.; Schick, M. Correlations in a Rigid–Flexible Diblock Copolymer System. *J. Chem. Phys.* **1992**, *96* (1), 730–739.
(12) Müller, M.; Schick, M. Ordered Phases in Rod−Coil Diblock Copolymers. *Macromolecules* **1996**, *29* (27), 8900–8903.
(13) Lin, S.-H.; Ho, C.-C.; Su, W.-F. Cylinder-to-Gyroid Phase Transition in a Rod–Coil Diblock Copolymer. *Soft Matter* **2012**, *8* (18), 4890–4893.
(14) Iovu, M. C.; Zhang, R.; Cooper, J. R.; Smilgies, D. M.; Javier, A. E.; Sheina, E. E.; Kowalewski, T.; McCullough, R. D. Conducting Block Copolymers of Regioregular Poly(3-Hexylthiophene) and Poly(Methacrylates): Electronic Materials with Variable Conductivities and Degrees of Interfibrillar Order. *Macromol. Rapid Commun.* **2007**, *28* (17), 1816–1824.
(15) Stefan, M. C.; Bhatt, M. P.; Sista, P.; Magurudeniya, H. D. Grignard Metathesis (GRIM) Polymerization for the Synthesis of Conjugated Block Copolymers Containing Regioregular Poly(3-Hexylthiophene). *Polym Chem* **2012**, *3* (7), 1693–1701.
(16) Alemseghed, M. G.; Servello, J.; Hundt, N.; Sista, P.; Biewer, M. C.; Stefan, M. C. Amphiphilic Block Copolymers Containing Regioregular Poly(3-Hexylthiophene) and Poly(2-Ethyl-2-Oxazoline). *Macromol. Chem. Phys.* **2010**, *211* (12), 1291–1297.
(17) Erothu, H.; Kolomanska, J.; Johnston, P.; Schumann, S.; Deribew, D.; Toolan, D. T. W.; Gregori, A.; Dagron-Lartigau, C.; Portale, G.; Bras, W.; Arnold, T.; Distler, A.; Hiorns, R. C.; Mokarian-Tabari, P.; Collins, T. W.; Howse, J. R.; Topham, P. D. Synthesis, Thermal Processing, and Thin Film Morphology of Poly(3-Hexylthiophene)–Poly(Styrenesulfonate) Block Copolymers. *Macromolecules* **2015**, *48* (7), 2107–2117.
(18) Javier, A. E.; Patel, S. N.; Hallinan, D. T.; Srinivasan, V.; Balsara, N. P. Simultaneous Electronic and Ionic Conduction in a Block Copolymer: Application in Lithium Battery Electrodes. *Angew. Chem. Int. Ed.* **2011**, *50* (42), 9848–9851.

(19) Lee, Y.-H.; Yen, W.-C.; Su, W.-F.; Dai, C.-A. Self-Assembly and Phase Transformations of π-Conjugated Block Copolymers That Bend and Twist: From Rigid-Rod Nanowires to Highly Curvaceous Gyroids. *Soft Matter* **2011**, *7* (21), 10429–10442.
(20) Lee, Y.-H.; Yang, Y.-L.; Yen, W.-C.; Su, W.-F.; Dai, C.-A. Solution Self-Assembly and Phase Transformations of Form II Crystals in Nanoconfined Poly(3-Hexyl Thiophene) Based Rod-Coil Block Copolymers. *Nanoscale* **2014**, *6* (4), 2194–2200.
(21) Lin, S.-H.; Wu, S.-J.; Ho, C.-C.; Su, W.-F. Rational Design of Versatile Self-Assembly Morphology of Rod–Coil Block Copolymer. *Macromolecules* **2013**, *46* (7), 2725–2732.
(22) Ji, E.; Pellerin, V.; Rubatat, L.; Grelet, E.; Bousquet, A.; Billon, L. Self-Assembly of Ionizable "Clicked" P3HT-b-PMMA Copolymers: Ionic Bonding Group/Counterion Effects on Morphology. *Macromolecules* **2017**, *50* (1), 235–243.
(23) Ji, E.; Pellerin, V.; Ehrenfeld, F.; Laffore, A.; Bousquet, A.; Billon, L. Hierarchical Honeycomb-Structured Films by Directed Self-Assembly in "Breath Figure" Templating of Ionizable "Clicked" PH3T-b-PMMA Diblock Copolymers: An Ionic Group/Counter-Ion Effect on Porous Polymer Film Morphology. *Chem. Commun.* **2017**, *53* (11), 1876–1879.
(24) Gaines, M. K.; Smith, S. D.; Samseth, J.; Bockstaller, M. R.; Thompson, R. B.; Rasmussen, K. Ø.; Spontak, R. J. Nanoparticle-Regulated Phase Behavior of Ordered Block Copolymers. *Soft Matter* **2008**, *4* (8), 1609–1612.
(25) Chiu, J. J.; Kim, B. J.; Kramer, E. J.; Pine, D. J. Control of Nanoparticle Location in Block Copolymers. *J. Am. Chem. Soc.* **2005**, *127* (14), 5036–5037.
(26) Kang, H.; Detcheverry, F. A.; Mangham, A. N.; Stoykovich, M. P.; Daoulas, K. C.; Hamers, R. J.; Müller, M.; De Pablo, J. J.; Nealey, P. F. Hierarchical assembly of nanoparticle superstructures from block copolymer-nanoparticle composites. *Phys. Rev. Lett.* **2008**, *100* (14), 148303–148307.
(27) Chiu, J. J.; Kim, B. J.; Yi, G.-R.; Bang, J.; Kramer, E. J.; Pine, D. J. Distribution of Nanoparticles in Lamellar Domains of Block Copolymers. *Macromolecules* **2007**, *40* (9), 3361–3365.
(28) Kuila, B. K.; Formanek, P.; Stamm, M. Multilayer Polymer Thin Films for Fabrication of Ordered Multifunctional Polymer Nanocomposites. *Nanoscale* **2013**, *5* (22), 10849.
(29) Liao, F.; Shi, L.-Y.; Cheng, L.-C.; Lee, S.; Ran, R.; Yager, K. G.; Ross, C. A. Self-Assembly of a Silicon-Containing Side-Chain Liquid Crystalline Block Copolymer in Bulk and in Thin Films: Kinetic Pathway of a Cylinder to Sphere Transition. *Nanoscale* **2018**, *11* (1), 285–293.
(30) Park, H.; Kim, J.-U.; Park, S. High-Throughput Preparation of Complex Multi-Scale Patterns from Block Copolymer/Homopolymer Blend Films. *Nanoscale* **2012**, *4* (4), 1362.
(31) Balazs, A. C.; Emrick, T.; Russell, T. P. Nanoparticle Polymer Composites: Where Two Small Worlds Meet. *Science* **2006**, *314* (5802), 1107–1110.
(32) Mezzenga, R.; Ruokolainen, J. Nanocomposites: Nanoparticles in the Right Place. *Nat. Mater.* **2009**, *8* (12), 926–928.
(33) Hoheisel, T. N.; Hur, K.; Wiesner, U. B. Block Copolymer-Nanoparticle Hybrid Self-Assembly. *Prog. Polym. Sci.* **2015**, *40*, 3–32.
(34) Kao, J.; Thorkelsson, K.; Bai, P.; Rancatore, B. J.; Xu, T. Toward Functional Nanocomposites: Taking the Best of Nanoparticles, Polymers, and Small Molecules. *Chem. Soc. Rev.* **2013**, *42* (7), 2654–2678.

(35) Lin, Y.; Daga, V. K.; Anderson, E. R.; Gido, S. P.; Watkins, J. J. Nanoparticle-Driven Assembly of Block Copolymers: A Simple Route to Ordered Hybrid Materials. *J. Am. Chem. Soc.* **2011**, *133* (17), 6513–6516.
(36) Jang, S. G.; Khan, A.; Hawker, C. J.; Kramer, E. J. Morphology Evolution of PS- *b* -P2VP Diblock Copolymers via Supramolecular Assembly of Hydroxylated Gold Nanoparticles. *Macromolecules* **2012**, *45* (3), 1553–1561.
(37) Voet, V. S. D.; Tichelaar, M.; Tanase, S.; Mittelmeijer-Hazeleger, M. C.; Brinke, G. ten; Loos, K. Poly(Vinylidene Fluoride)/Nickel Nanocomposites from Semicrystalline Block Copolymer Precursors. *Nanoscale* **2012**, *5* (1), 184–192.
(38) Bockstaller, M. R.; Lapetnikov, Y.; Margel, S.; Thomas, E. L. Size-Selective Organization of Enthalpic Compatibilized Nanocrystals in Ternary Block Copolymer/Particle Mixtures. *J. Am. Chem. Soc.* **2003**, *125* (18), 5276–5277.
(39) Spontak, R. J.; Shankar, R.; Bowman, M. K.; Krishnan, A. S.; Hamersky, M. W.; Samseth, J.; Bockstaller, M. R.; Rasmussen, K. Ø. Selectivity- and Size-Induced Segregation of Molecular and Nanoscale Species in Microphase-Ordered Triblock Copolymers. *Nano Lett.* **2006**, *6* (9), 2115–2120.
(40) Terzić, I.; Meereboer, N. L.; Mellema, H. H.; Loos, K. Polymer-Based Multiferroic Nanocomposites via Directed Block Copolymer Self-Assembly. *J. Mater. Chem. C* **2019**, *7* (4), 968–976.
(41) Yeh, S.-W.; Wei, K.-H.; Sun, Y.-S.; Jeng, U.-S.; Liang, K. S. CdS Nanoparticles Induce a Morphological Transformation of Poly(Styrene-b-4-Vinylpyridine) from Hexagonally Packed Cylinders to a Lamellar Structure. *Macromolecules* **2005**, *38* (15), 6559–6565.
(42) Lee, H.; Lee, E.; Kim, D. K.; Jang, N. K.; Jeong, Y. Y.; Jon, S. Antibiofouling Polymer-Coated Superparamagnetic Iron Oxide Nanoparticles as Potential Magnetic Resonance Contrast Agents for in Vivo Cancer Imaging. *J. Am. Chem. Soc.* **2006**, *128* (22), 7383–7389.
(43) Hu; Neoh, K. G.; Cen, L.; Kang, E.-T. Cellular Response to Magnetic Nanoparticles "PEGylated" via Surface-Initiated Atom Transfer Radical Polymerization. *Biomacromolecules* **2006**, *7* (3), 809–816. https://doi.org/10.1021/bm050870e.
(44) Bontempo, D.; Maynard, H. D. Streptavidin as a Macroinitiator for Polymerization: In Situ Protein−Polymer Conjugate Formation. *J. Am. Chem. Soc.* **2005**, *127* (18), 6508–6509.
(45) Scofield, J. H. Hartree-Slater Subshell Photoionization Cross-Sections at 1254 and 1487 EV. *J. Electron Spectrosc. Relat. Phenom.* **1976**, *8* (2), 129–137.
(46) Awada, H.; Medlej, H.; Blanc, S.; Delville, M.-H.; Hiorns, R. C.; Bousquet, A.; Dagron-Lartigau, C.; Billon, L. Versatile Functional Poly(3-Hexylthiophene) for Hybrid Particles Synthesis by the Grafting onto Technique: Core@shell ZnO Nanorods. *J. Polym. Sci. Part Polym. Chem.* **2014**, *52* (1), 30–38.
(47) Jana, N. R.; Gearheart, L.; Murphy, C. J. Seed-Mediated Growth Approach for Shape-Controlled Synthesis of Spheroidal and Rod-like Gold Nanoparticles Using a Surfactant Template. *Adv. Mater.* **2001**, *13* (18), 1389–1393.
(48) Sumerlin, B. S.; Vogt, A. P. Macromolecular Engineering through Click Chemistry and Other Efficient Transformations. *Macromolecules* **2010**, *43* (1), 1–13.
(49) Mehtala, J. G.; Zemlyanov, D. Y.; Max, J. P.; Kadasala, N.; Zhao, S.; Wei, A. Citrate-Stabilized Gold Nanorods. *Langmuir* **2014**, *30* (46), 13727–13730.

(50) Mikhlin, Y. L.; Vorobyev, S. A.; Saikova, S. V.; Vishnyakova, E. A.; Romanchenko, A. S.; Zharkov, S. M.; Larichev, Y. V. On the Nature of Citrate-Derived Surface Species on Ag Nanoparticles: Insights from X-Ray Photoelectron Spectroscopy. *Appl. Surf. Sci.* **2018**, *427*, 687–694.
(51) Mazov, I.; Kuznetsov, V. L.; Simonova, I. A.; Stadnichenko, A. I.; Ishchenko, A. V.; Romanenko, A. I.; Tkachev, E. N.; Anikeeva, O. B. Oxidation Behavior of Multiwall Carbon Nanotubes with Different Diameters and Morphology. *Appl. Surf. Sci.* **2012**, *258* (17), 6272–6280.
(52) Okpalugo, T. I. T.; Papakonstantinou, P.; Murphy, H.; McLaughlin, J.; Brown, N. M. D. High Resolution XPS Characterization of Chemical Functionalised MWCNTs and SWCNTs. *Carbon* **2005**, *43* (1), 153–161.
(53) Huang, D.; Cui, J.; Chen, X. A Morpholinium Surfactant Crystallization Induced Formation of Au Nanoparticle Sheet-like Assemblies with Uniform SERS Activity. *Colloids Surf. Physicochem. Eng. Asp.* **2014**, *456*, 100–107.
(54) Lachkar, A.; Selmani, A.; Sacher, E.; Leclerc, M. Metallization of Polythiophenes IV. Interaction of Vapor-Deposited Cu and Ni with Poly[3-(1,1,1,2,2,3,3,4,4,5,5,6,6-Tridecafluorononyl)Thiophene] (P3TT). *Synth. Met.* **1995**, *75* (3), 195–200.
(55) Kim, B. J.; Bang, J.; Hawker, C. J.; Kramer, E. J. Effect of Areal Chain Density on the Location of Polymer-Modified Gold Nanoparticles in a Block Copolymer Template. *Macromolecules* **2006**, *39* (12), 4108–4114.
(56) Martin-Vosshage, D.; Chowdari, B. V. R. X-Ray Photoelectron Spectroscopy Studies on PEOnMBr2 (M = Co, Ni, Zn) Solid Electrolytes. *Solid State Ion.* **1995**, *78* (1), 9–17.
(57) Hearn, M. J.; Briggs, D. Analysis of Polymer Surfaces by SIMS. 12. On the Fragmentation of Acrylic and Methacrylic Homopolymers and the Interpretation of Their Positive and Negative Ion Spectra. *Surf. Interface Anal.* **1988**, *11* (4), 198–213.
(58) Hearn, M. J.; Ratner, B. D.; Briggs, D. SIMS and XPS Studies of Polyurethane Surfaces. 1. Preliminary Studies. *Macromolecules* **1988**, *21* (10), 2950–2959.
(59) Dai, C.-A.; Yen, W.-C.; Lee, Y.-H.; Ho, C.-C.; Su, W.-F. Facile Synthesis of Well-Defined Block Copolymers Containing Regioregular Poly(3-Hexyl Thiophene) via Anionic Macroinitiation Method and Their Self-Assembly Behavior. *J. Am. Chem. Soc.* **2007**, *129* (36), 11036–11038.
(60) Lutz, J.-F. Polymerization of Oligo(Ethylene Glycol) (Meth)Acrylates: Toward New Generations of Smart Biocompatible Materials. *J. Polym. Sci. Part Polym. Chem.* **2008**, *46* (11), 3459–3470.
(61) Lutz, J.-F.; Weichenhan, K.; Akdemir, Ö.; Hoth, A. About the Phase Transitions in Aqueous Solutions of Thermoresponsive Copolymers and Hydrogels Based on 2-(2-Methoxyethoxy)Ethyl Methacrylate and Oligo(Ethylene Glycol) Methacrylate. *Macromolecules* **2007**, *40* (7), 2503–2508.
(62) Aguirre, G.; Khoukh, A.; Chougrani, K.; Alard, V.; Billon, L. Dual-Responsive Biocompatible Microgels as High Loaded Cargo: Understanding of Encapsulation/Release Driving Forces by NMR NOESY. *Polym. Chem.* **2018**, *9* (6), 757–768.
(63) Aguirre, G.; Khoukh, A.; Taboada, P.; Chougrani, K.; Alard, V.; Billon, L. Smart Self-Assembled Microgel Films as Encapsulating Carriers for UV-Absorbing Molecules. *Polym. Chem.* **2018**, *9* (10), 1155–1159.

(64) Aguirre, G.; Deniau, E.; Brûlet, A.; Chougrani, K.; Alard, V.; Billon, L. Versatile Oligo(Ethylene Glycol)-Based Biocompatible Microgels for Loading/Release of Active Bio(Macro)Molecules. *Colloids Surf. B Biointerfaces* **2019**, *175*, 445–453.

"For Table of Contents Use Only."